inorganics

MDPI

Article

First Principles Study of Electronic and Optical Properties of Cadmium-Tin-Oxide

Adel Bandar Alruqi

Department of Physics, Faculty of Science, King Abdulaziz University, Jeddah 21589, Saudi Arabia; aalruqi@kau.edu.sa

Abstract: Cadmium-tin-oxide (CTO), also referred to as cadmium stannate (Cd_2SnO_4), is known for its interesting electrical, electronic, and optical properties, making it useful in various applications such as in transparent conducting oxides for optoelectronic devices and also in photovoltaic applications. While its properties have been investigated experimentally, there is not much record in the literature on the computational study of the electronic and optical properties of CTO. This study employed density functional theory to explore the two properties of CTO. The hybrid functionals were used to widen the band gap from 0.381 eV (for PBE) to 3.13 eV, which replicates the experimental values very well. The other properties obtained were a refractive index of 2.53, absorption coefficient of 1.43×10^4 cm^{-1}, and dielectric constant of 6.401 eV. The optical energy loss of 0.00691 that was investigated for the first time in this work adds to the literature on the properties of CTO. However, the electrical properties of CTO, which also play a key role in the working of optoelectronic devices, need to be investigated.

Keywords: cadmium stannate; absorption coefficient of cadmium-tin-oxide; band gap of cadmium-tin-oxide; dielectric constant of cadmium-tin-oxide; refractive index of cadmium-tin-oxide; band structure of cadmium-tin-oxide

1. Introduction

Cadmium-tin-oxide (CTO) is widely used in numerous applications as a transparent conducting oxide (TCO), especially in electronics and optoelectronics [1–3]. It is a useful material for applications requiring low resistivities and high electron mobility due to its low resistivity, high electron and hole mobilities, and low free-carrier absorption. Moreover, it conducts electricity while remaining transparent, a property which qualifies it for applications where both optical transparency and electrical conductivity are crucial.

CTO is now mostly utilized in thin-film solar cells, often as a transparent conducting layer that aids in the collection and transfer of electrical charge; in the manufacturing of liquid crystal displays and other flat panel displays; in the production of transparent conductive films for electronic device touchscreens; and in light-emitting diodes (where it can be employed as a transparent electrode) [4]. The desirable properties of CTO include its high electrical conductivity of up to 6500 Ω^{-1} cm^{-1}, optical transparency (due to its wide bandgap of approximately 3 eV), high absorption coefficient of above 2×10^4 cm^{-1}, and high transmittance to visible light of above 80% in the visible spectral wavelength (which make these applications possible) [5–7].

Physical vapor deposition (PVD) and chemical vapor deposition (CVD) are the two most popular methods for depositing thin films of CTO. In both processes, volatile precursors undergo chemical reactions to create a solid CTO on the substrate's surface. In order

check for updates

Academic Editor: Xiangrong Chen

Received: 13 November 2024
Revised: 24 December 2024
Accepted: 31 December 2024
Published: 7 January 2025

Citation: Alruqi, A.B. First Principles Study of Electronic and Optical Properties of Cadmium-Tin-Oxide. *Inorganics* **2025**, *13*, 14. https://doi.org/10.3390/inorganics13010014

Copyright: © 2025 by the author. Licensee MDPI, Basel, Switzerland. This article is an open access article distributed under the terms and conditions of the Creative Commons Attribution (CC BY) license (https://creativecommons.org/licenses/by/4.0/).

to promote the reaction and thin-film deposition, the substrate is usually heated. Examples of CVD methods include spray pyrolysis [6,8], sol-gel, and chemical co-precipitation [9]. In contrast, PVD is a thin film deposition method in which a material is evaporated in a vacuum before condensing into a thin film onto a substrate. The process takes place in a vacuum chamber in order to reduce interference from the surrounding atmosphere. PVD is widely used for applications requiring thin films with specific properties such as improved hardness, wear resistance, and optical properties. The PVD methods include evaporation, ion plating, and sputtering (magnetron sputtering and radio frequency magnetron sputtering) [10,11].

The literature shows that although the thermodynamics as well as the mechanics of CTO have been extensively investigated by ab initio methods [12,13], its electronic and optical properties have mainly been investigated using experimental methods through the deposition of the films of the material on glass (normal microscope, borosilicate, and Corning) as a substrate [14,15]. A recent computational study that investigated the electrical properties of CTO employed the *VASP* package and the GGA + U method [16]. The current work examined the optical and electronic properties of CTO using a different method as well as a different functional (the *Quantum Espresso* package and the Heyd-Scuseria-Ernzerhof (HSE) functional), primarily attempting to compare the computed values with published experimental values. Moreover, this study attempted to calculate the optical energy loss for the first time, with the aim of enriching the current literature on the properties of CTO. The main shortcoming of the ab initio calculations of underestimating the bandgap was addressed by employing the HSE hybrid functional.

2. Results and Discussion

2.1. Structural Properties

Before presenting the electronic and optical properties of CTO, its structural properties were first investigated in order to determine the relaxed unit cell parameters. Structural properties refer to the characteristics and attributes of a material or system that describe its physical arrangement, organization, and behavior at the atomic, molecular, or macroscopic levels [17]. Table 1 presents the computed lattice constants, the density of CTO, as well as a comparison with some literature values. It was discovered that there is excellent agreement between the computed values of the lattice parameters and the density of CTO and the experimental values reported in the literature.

Table 1. The estimated density and lattice constants of cadmium-tin-oxide.

Parameter	a (Å)	b (Å)	c (Å)	ρ kg/m^3
This work	5.57 ± 0.06	9.9 ± 0.1	3.21 ± 0.02	7632.6 ± 8
Others	5.568 [18], 5.568 [19]	9.894 [18], 9.895 [19]	3.193 [18], 3.194 [19]	7680.52 [20]

All the calculated lattice parameter values were found to be less than 1% of the literature values, although the known trend of the overestimation of the lattice parameters by the generalized gradient approximation (GGA) was witnessed. A lower density of 0.6239% compared to the result from the study by Troemel [20] was obtained, which can be attributed to the higher lattice parameters computed in this work.

2.2. Electronic Properties

Important details regarding the distribution of electrons within a material and their behavior when exposed to external stimuli, like an electric field, can be found in the band structure [21]. The band structure, PDOS, and TDOS of CTO are shown in Figure 1a, which shows that both the conduction band maximum (CBM) and the valence band maximum

(VBM) are located at the Y point. Thus, a direct band gap of CTO is observed at the Y-Y point in this study. A computational study of orthorhombic CTO by Tang et al. [16] also reported a direct band gap of CTO, but at the Γ point. However, unlike earlier studies on the band structure of CTO (both experimental and computational) that have obtained band gaps of between 2.6 and 3.81 eV [22–24], the calculated value in this study using the PBE functional is just 0.381 eV, which is way too low. This is a known trend of the local and semilocal exchange correlation (XC) functionals that seriously underestimate the band gap [25,26]. The inclusion of the GGA-HSE hybrid XC functional improved the value of the band gap tremendously (Table 2), leading to a value comparable to the experimental values in the literature [22–24], presenting 16.04% above the value reported by Ravera and Sharma [22] and 21.61% above the maximum value obtained by Zhu et al. [24]. The computed HSE band gap is very close (2.14%) to the maximum value reported by Lakshmi et al. [23]. The study by Ravera and Sharma [22] used dip coating as the method of deposition, while the band gap measurement was determined using the Van der Pauw technique. In the study by Lakshmi et al. [23], chemical vapor deposition was employed, and the band gap was determined using the Tauc relation; while Zhu et al. [24] used sputtering to deposit the thin films of CTO, and the band gap was determined using the Tauc relation. Hybrid functionals improve the prediction of band gaps by incorporating a fraction of Hartree–Fock exchange energy, which helps to better capture electron correlation effects, reduce self-interaction errors, and improve the description of delocalized electrons and excited states.

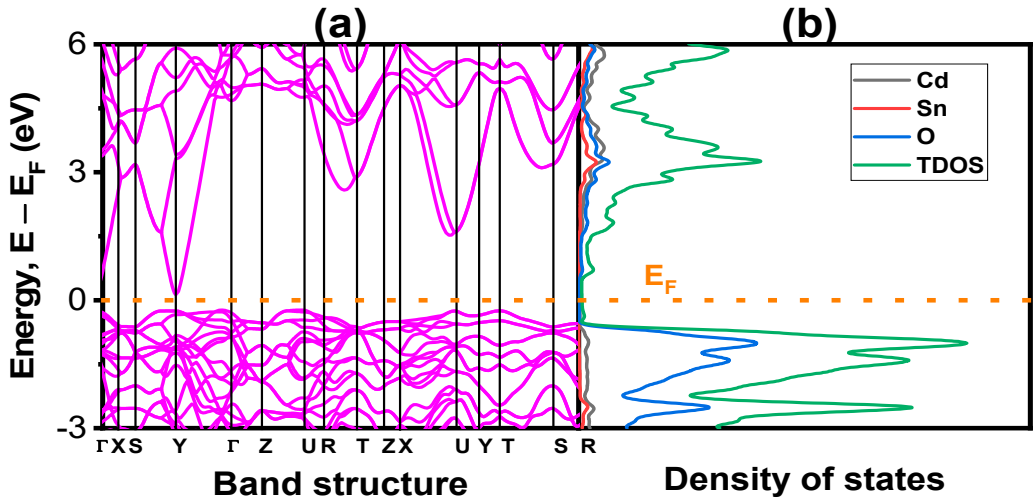


Figure 1. The electronic properties of cadmium-tin-oxide showing (**a**) the band structure and (**b**) the density of states.

However, it is worthwhile to note that the fraction of exact exchange included in the HSE functional (commonly 25%) is semi-empirical. While this value works well for many materials, it might not be optimal for all systems, leading to inaccuracies in band gap prediction for certain materials, especially those with unusual electronic properties. Moreover, HSE struggles with systems where the electronic states are highly localized or exhibit strong correlation effects (such as transition metal oxides, lanthanides, and actinides), in addition to being significantly more computationally expensive [27]. The computed band gap obtained in this study also compares well with the value reported by Tang, Shang, and Zhang [16] at 3.0 eV, with the deviation being attributed to the different computational techniques used. The study by Tang, Shang, and Zhang employed the *VASP* package with GGA + U, while the present study used *Quantum Espresso* (version 6.4.1), with HSE. The position of the Fermi energy level (E_F) shown in Figures 1 and 2 was obtained from the non-consistent field (nscf) calculation.

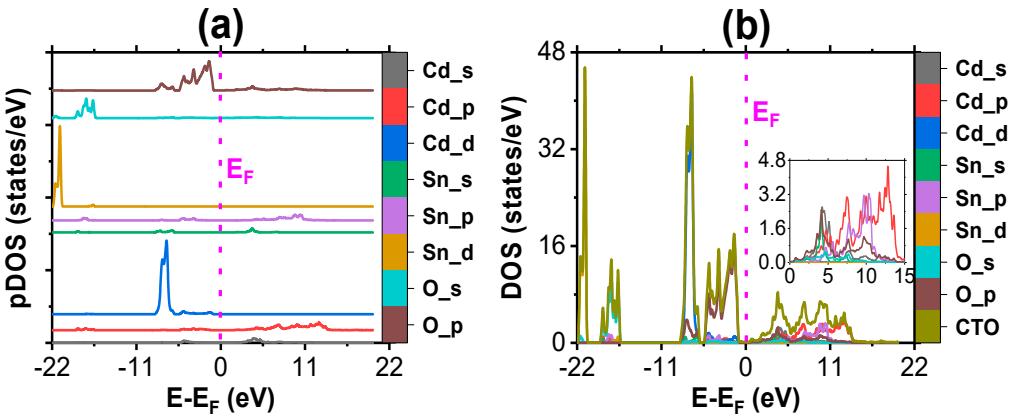


Figure 2. Density of states of cadmium-tin-oxide: (**a**) Projected DOS, and (**b**) Effective DOS.

Table 2. The calculated cadmium-tin-oxide band gap, dielectric constant, refractive index, absorption coefficient, and optical energy loss, together with some values in the literature.

Constant	E_g (eV)	ε (eV)	n	α ($\times 10^4$ cm^{-1})	L (ω)
This study	0.381 ± 0.003-GGA 3.13 ± 0.03-HSE	6.40 ± 0.06	2.53 ± 0.02	1.43 ± 0.01	0.00691
Others	2.7 [22], 2.6–3.2 [23], 3.75–3.81 [24]	———	2.6 [28], 2.108–3.542 [6]	1.399 [6]	———

The density of states (DOS) is a fundamental property that influences various electronic and optical properties of materials. Figure 1b depicts the overall DOS for CTO calculated using the normal PBE functional, which clearly indicates that the VB is dominated by the O-states, while the Cd and Sn states make minimal contributions. The CB, however, is dominated by an overlap of the Cd and O states, with Sn having a small contribution. Since the VB maximum and CB minimum involve the same momentum, efficient optical transitions occur, which is important in optoelectronics. Figure 2a, which depicts the partial DOS (PDOS) of CTO, shows that the VB is made up of the O-p, O-s, Sn-d, and Cd-d states. The O-s and Sn-d states are located deeper in the VB, giving rise to features at around −17 eV and −21 eV, respectively. The sharp feature observed at around −7 eV is contributed mainly by the Cd-d orbital, with very minimal contribution from the O-p orbital.

Figure 2a,b demonstrate that the O-s states dominate the VB edge, with the remaining states contributing very little. On the other hand, the CB's orbital contribution is not clearly dominant. However, as can be seen in both Figure 2a and the zoomed-in portion of Figure 2b, the Cd-p and Sn-p states are located deep within the CB, whilst the O-p, Cd-s, and Sn-s states dominate the CB edge. The Cd-p and Sn-p states deep within the CB overlap, as do the O-p, Cd-s, and Sn-s states at the CB edge. The curvature of the bands (which relates to the effective mass of carriers) depends on the dominant states. The highly delocalized states (the s-orbitals) observed in this study show low effective mass and therefore, high mobility. Moreover, the nature of the dominant states affects the material's tolerance to defects and impurities. If the VB or CB is dominated by states with significant overlap (delocalized), the material tends to be more defect-tolerant. Thus, since there are overlaps in the Cd-p and Sn-p states as well as the O-p, Cd-s, and Sn-s states, CTO is more defect-tolerant, making it more resilient to disruptions that would typically degrade its performance, such as point defects, vacancies, interstitials, or grain boundaries. The flat bands located deep within the VB are mostly caused by non-bonding Sn-s orbitals (with little overlap).

2.3. Optical Properties

A material's optical properties can be inferred from its dielectric function (which is linked to its electrical structure). It is especially crucial for comprehending how materials respond to light [29]. The dielectric function, depicted in Figure 3, has many peaks associated with band-to-band transitions. The figures show that the imaginary part of the dielectric constant has a peak at and an energy of 1.5 eV and then dies off thereafter, which is in contrast to the result reported by Tang et al. [16], which showed a general increase with the increase in the energy. The disparity between the two curves can be attributed to the different computational methods employed. Tang et al. used PAW pseudopotentials within the *VASP* package, while this study used PBE pseudopotentials within the *Quantum Espresso* package (version 6.4.1). As energy increases, the dielectric function's peaks disappear, and this is a characteristic feature observed in many materials, which is often associated with electronic transitions within the material. The effect of the disappearance of the peak of the dielectric function with energy is responsible for the phenomenon whereby higher energy levels are involved in transitions that may become likely or occur less frequently with the increase in the energy of the incoming light. Furthermore, the energy of the scattered or absorbed photon must equal the energy needed for the electronic transition due to the principle of conservation of energy. At higher energies, there may be fewer electronic states available for absorption, leading to a reduction in the intensity of absorption peaks, which is evident in Figure 3 at frequencies above 5 eV. Materials often exhibit multiple electronic processes contributing to the dielectric function. At higher energies, additional electronic processes may come into play, leading to the redistribution of the overall spectral intensity. The effect can also be brought about by the bandwidth effects. At higher energies, electronic transitions tend to have broader bandwidths, resulting in peaks that are less sharp and more spread-out [30].

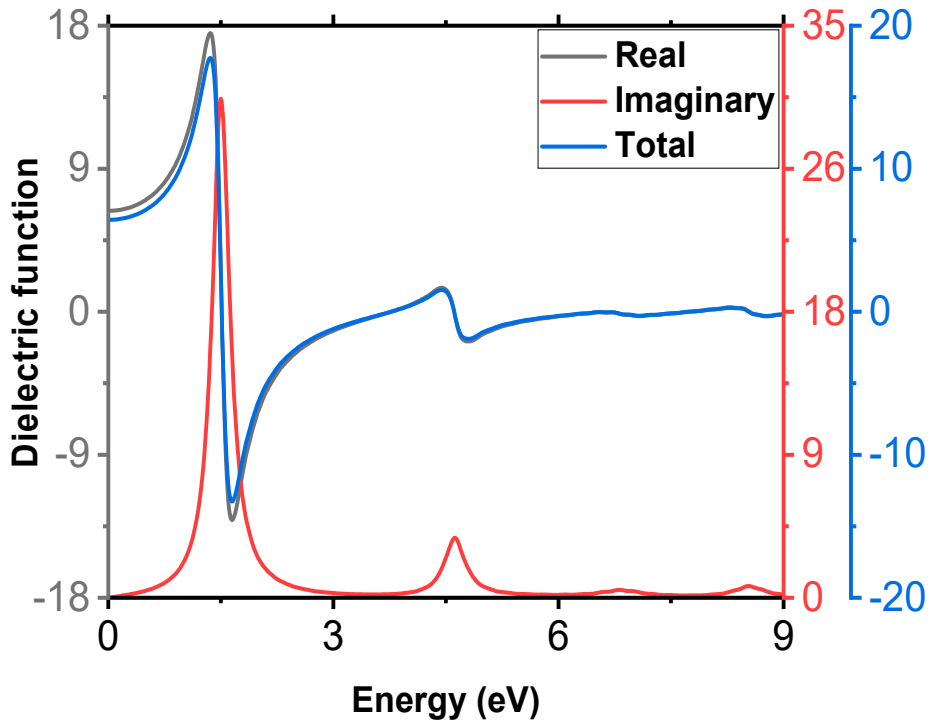


Figure 3. The real part, imaginary part, and effective dielectric function.

Two major peaks are observed in Figure 3 at 1.64 eV and 4.76 eV for the real part of the dielectric function and at 1.51 eV and 4.63 eV for the imaginary part, both of which show an energy difference of 3.12 eV, which implies the occurrence of electronic transition at

this energy. The important part of the dielectric function is the static dielectric constant (ε), which depends on the bandgap energy, and is equal to the square of the refractive index (n). ε is obtained at the origin of the dielectric function, and its extracted value for CTO is shown in Table 2, which is within the range for semiconductors at 3–35 [31]. ε is a fundamental property of materials that describes their ability to store electrical energy in an electric field. Materials with higher dielectric constants offer significant advantages in terms of increased capacitance, energy storage capacity, signal integrity, insulation, and tunability, making them essential components in a wide range of electronic, electrical, and optical devices and systems. Since the dielectric constant of CTO at 6.401 is considered low for semiconductors, it implies that CTO is not ideal for the applications mentioned above. This value is, however, comparable to that of the cubic CTO ($CdSnO_3$) at 4.62 [32] and indium tin oxide (ITO, one of the commonly used transparent conducting oxides in touchscreens (smartphones and tablets), flat-panel displays (LCD, OLED, and plasma screens), and solar cells (as transparent electrodes in photovoltaic devices), which has a value of 8.7 [33].

The refractive index indicates how light travels through a material. It is critical in the design of optical components such as lenses, prisms, and fibers [34,35]. In Figure 4, it can be observed that the refractive index decreases as the energy increases. This is a common phenomenon in many materials, especially the transparent ones, where the refractive index is wavelength-dependent, and has also been observed in previous studies [6,22]. The behavior is known as normal or positive dispersion, and it can be brought about by a number of factors, including electronic resonances, energy level transitions, and material absorption bands. At higher energies of ultraviolet and beyond, the electronic resonances and transitions within the material may result in a decrease in the refractive index, which is often observed as the material absorbs more light in these higher energy ranges. Electronic transitions associated with higher energy levels can lead to a rise in the absorption of light, which, in effect, reduces the effective speed of light within the material, resulting in a lower refractive index.

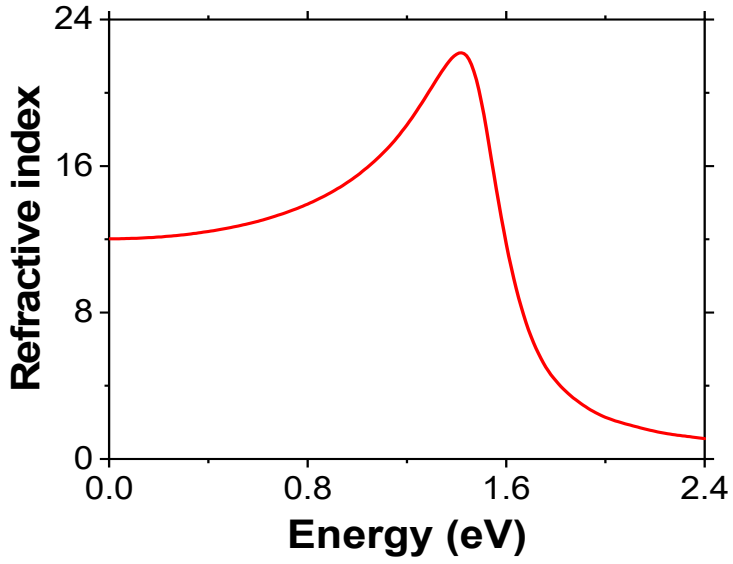


Figure 4. The calculated refractive index as a function of energy.

The peak of the refractive index in this study was obtained at the 873 nm (UV) wavelength, which corresponds to an energy of 1.42 eV. Common materials have refractive indices that are greater than 1, with the majority lying between 1.3 to 1.7. Silicon has the highest value at 3.88, while diamond and lithium niobate have 2.4 and 2.2, respectively [35,36]. The calculated value of the refractive index in this work therefore falls in the class of materials with high refractive indices, with the value being in accord with the

literature values (Table 2). The value of the refractive index was obtained at the 633 nm wavelength (corresponding to an energy of 1.96 eV). A high refractive index is a significant optical property with various practical implications in science, technology, and everyday applications, such as in the design and manufacturing of optical devices and components. These materials allow for the more efficient bending and focusing of light, contributing to the performance of optical systems. High-refractive-index materials are also essential in the field of photonics and optoelectronics. In devices like optical fibers and waveguides, materials with high refractive indices enable efficient light confinement and transmission. This is particularly important for applications in telecommunications and data transmission. Furthermore, high-refractive-index materials are used in the construction of microscope objectives and imaging optics. They play a crucial role in achieving high-resolution imaging by minimizing distortions and improving light-gathering capabilities [37]. CTO is therefore a prime candidate in the aforementioned applications.

Figure 5 depicts the variation of the absorption coefficient with the wavelength, which indicates an increase as the wavelength increases. This is in contrast to the result reported by Tang et al. [16], which shows a decrease, and the disparity between the two can be attributed to the different computational methods employed. Materials' electronic structures and the types of transitions that result in absorption dictate the relationship between the optical absorption coefficient and wavelength. The type of bandgap and the density of states are the two common causes of this behavior, though it can also vary based on the particular properties of the material [38].

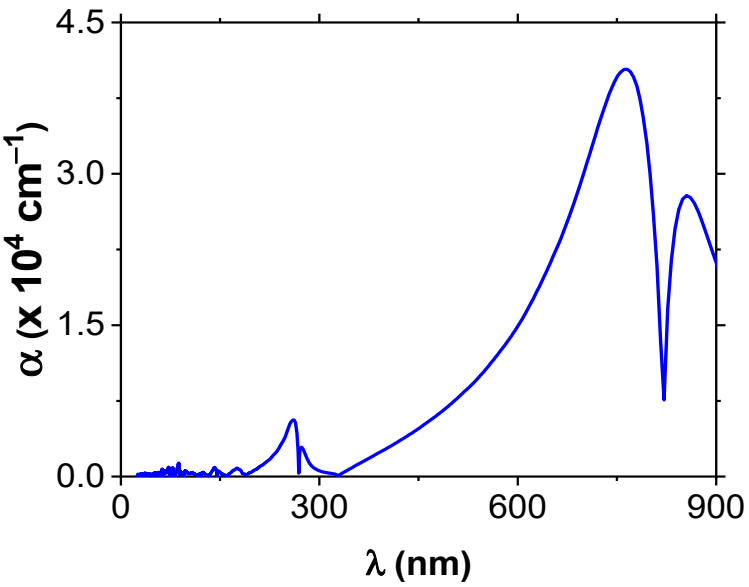


Figure 5. The computed optical absorption coefficient.

In materials with a direct bandgap, the absorption coefficient often decreases as energy increases beyond the bandgap. This is so because an electron is promoted from the valence band to the conduction band during a direct transition. Once this energy is surpassed, the absorption probability decreases. At lower energies, the absorption coefficient may increase as phonon-assisted transitions become more probable. However, at higher energies, the absorption coefficient tends to decrease. The density of electronic states in a material is an important factor. At lower energies, there might be a higher density of available states for absorption, leading to a higher absorption coefficient. As energy increases, the available electronic states become less dense, resulting in a decrease in the absorption coefficient [39].

The calculated value of the absorption coefficient shown in Table 2 agrees with the literature values. Previous works have reported that CTO has a large absorption coefficient,

with some reporting values in the order of $\times 10^5$ cm^{-1} at higher energies [40]. A high optical absorption coefficient in a material can have several significant implications and applications in various fields, including in photovoltaics, photodetectors and sensors, and thermal imaging. In the field of solar energy, a high optical absorption coefficient is crucial for the efficient absorption of sunlight. Photovoltaic materials with high absorption coefficients can capture a larger fraction of incident sunlight, leading to improved solar cell efficiency. In thermal imaging applications, materials with high absorption coefficients in the infrared range are desirable. Such materials effectively absorb thermal radiation, allowing for the creation of high-quality thermal images [41]. Thus, CTO is an attractive candidate in the aforementioned applications.

The loss of light energy or intensity during transmission through a medium is referred to as optical energy loss. As Figure 6 depicts, there is no noticeable energy absorption within the visible spectrum. The first peak is observed at an energy of 3.95 eV, which is within the ultraviolet range. A higher peak is observed at 7.97 eV, which is still within the ultraviolet range. The peaks imply the photoelectron excitation of collective electron oscillations and interband transitions. The computed optical energy loss is presented in Table 2, which is much higher than that of $SrTiO_3$ and Ti_2O_3 at 0.000239–0.000355 and 0.000230–0.001520, respectively [40]. However, since there are no literature values of CTO for comparison, this study forms the basis for future reference. In devices such as lasers, solar cells, light-emitting diodes, and optical fibers, minimizing optical energy loss is crucial for achieving high efficiency. Optical energy loss provides insights into electronic transitions, the band structure, and material properties such as band gaps, defect states, and excitonic effects. High optical energy loss through absorption or scattering reduces the overall performance of these devices, impacting their functionality and effectiveness. A high value of optical energy loss can also lead to signal degradation, reducing the signal-to-noise ratio and limiting the transmission distance and data rates. In solar cell technology, minimizing optical energy loss is essential for maximizing the efficiency of energy conversion from sunlight into electricity [42,43]. Thus, CTO's higher optical energy loss is not good for several applications, especially in solar cells.

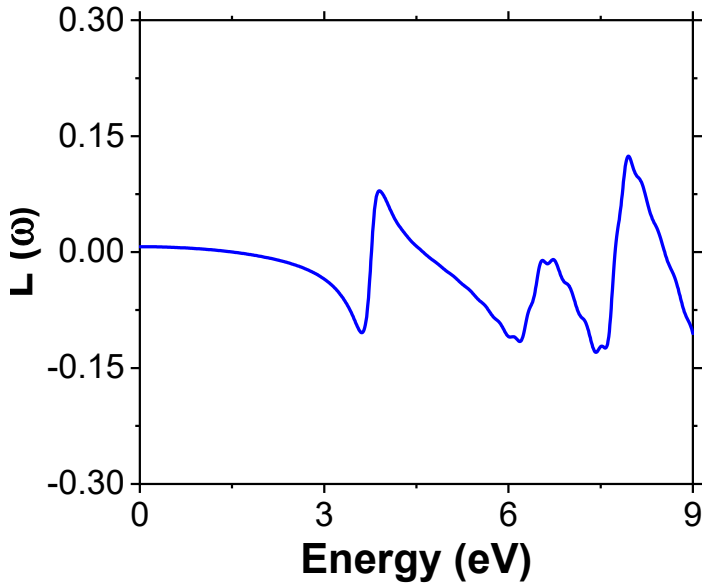


Figure 6. The calculated optical energy loss.

3. Materials and Methods

The open crystallographic database provided the crystallographic input file used in the investigation [44]. The three-dimensional structure of the CTO, an orthorhombic cell of

space group *pbam* (number 55), is depicted in Figure 7. The original parameters of the unit cell were $a = 5.665$ Å, $b = 10.127$ Å, and $c = 3.249$ Å. The unit cell was thereafter taken through structural optimization. The kinetic energy cut-off ecut was varied from 20 Ry to 90 Ry in steps of 10 Ry, while the k-points were varied from $2 \times 2 \times 2$ to $9 \times 9 \times 9$ in steps of $1 \times 1 \times 1$. The lattice parameters on the other hand, were varied from 5.099 to 6.232 Å for parameter a, 9.114 to 11.140 Å for parameter b, and 2.924 to 3.574 Å for parameter c. These values represent 10% below and above the reference values. The lattice point optimization was carried out using the Broyden–Fletcher–Goldfarb–Shanno (BFGS) algorithm, where the lattice positions were relaxed. The electronic and optical property calculations were then carried out on the relaxed structure. The density functional theory (DFT) within the *Quantum Espresso* package (version 6.4.1) was used for all of the computations [45], with the Perdew-Burke-Ernzerhof (PBE) exchange-correlation functionals (for both electronic and optical properties) and PBE-HSE functional (for electronic properties). Ultrasoft pseudopotentials were used. The optimized ecut was obtained at 50 Ry, and the charge density cut-off was set at 400 Ry (ecut $\times 8$ for ultrasoft pseudopotentials). An ideal Mokhorst-Pack k_point mesh [46] was established at dimensions of $5 \times 3 \times 9$ in the Brillouin zone.

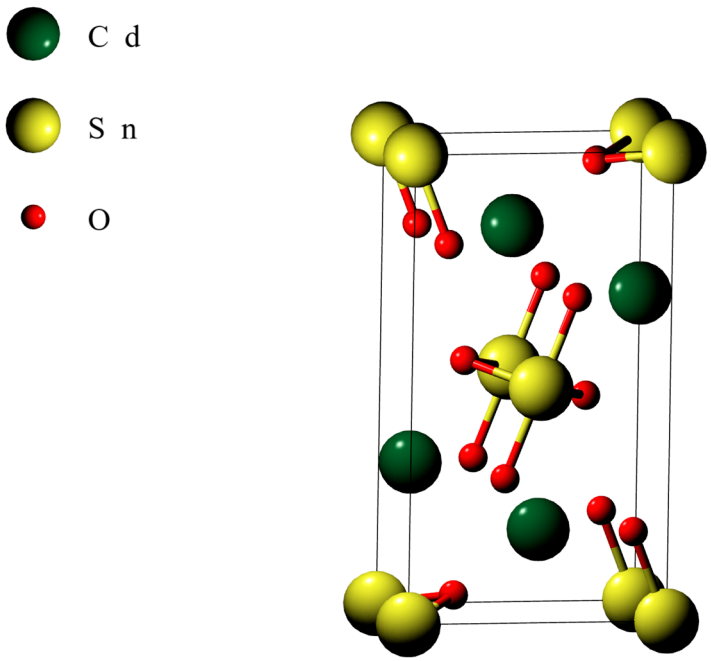


Figure 7. A 3D structure of cadmium-tin-oxide.

For the investigation of electronic properties, the HSE hybrid functional was invoked by including a 3D mesh for the q (k1 − k2) sampling of the Fock operator (EXX). The values were set as ***nqx*1=5, *nqx*2=3, *nqx*3=9**, which are the same as those of the k_point mesh. The parameters ***exxdiv_treatment="none"*** and ***x_gamma_extrapolation=.false.*** were set in the ***SYSTEM*** nameslist, since the study involved a non-cubic cell. The bandgap was determined by both the PBE and the PBE-HSE (hybrid) functionals. After determining the electronic structure and total energy of the system through the ground-state DFT calculation, the optical properties were calculated, which were implemented using time-dependent DFT (TDDFT), which involves exciting the system from its ground state by promoting electrons to higher energy orbitals. These excitations are associated with transitions between molecular orbitals. The real (ε_{re}) and imaginary (ε_{im}) components of the dielectric function (ε) were used to extract the frequency-dependent optical properties. The following relation-

ships were used to calculate the refractive index (n), the optical energy loss (L), and the absorption coefficient (α) [47,48]:

$$n = \frac{1}{\sqrt{2}}\sqrt{\sqrt{\varepsilon_{re}^2 + \varepsilon_{im}^2} + \varepsilon_{re}} \quad (1)$$

$$k = \frac{1}{\sqrt{2}}\sqrt{\sqrt{\varepsilon_{re}^2 + \varepsilon_{im}^2} - \varepsilon_{re}} \quad (2)$$

$$\alpha = \sqrt{2}\varepsilon\sqrt{\sqrt{\varepsilon_{re}^2 + \varepsilon_{im}^2} - \varepsilon_{re}} \quad (3)$$

$$L = \frac{\varepsilon_{re}}{\varepsilon_{re}^2 + \varepsilon_{im}^2} \quad (4)$$

The energy (E in eV) and wavelength (λ in nm) are related by

$$E = \frac{1239.8}{\lambda} \quad (5)$$

4. Conclusions

The study successfully investigated both the electronic and optical properties of CTO. It was discovered that the outcomes of the study and the values found in the literature agreed quite well. While the GGA seriously underestimated the bandgap (0.381 eV), GGA-HSE lead to a tremendous widening of the bandgap, reaching a value of 3.133 eV that is comparable to those from experiments. Both methods generated direct band gaps, which is in agreement with the results from the literature. An investigation of the DOS showed that the VB edge is dominated by the O-s orbitals, while the CB edge is dominated by the O-p, Cd-s, and Sn-s states. The computed refractive index of 2.53 is high, which is good for making microscope objectives and imaging optics. The high absorption coefficient of 1.43×10^4 cm^{-1} is good for solar cell efficiency. The computed value of the dielectric function of 6.401 is quite within the 3–35 range for semiconductors. However, the high optical energy loss of 0.00691 is not good, since it leads to signal degradation in opto-electronic devices. The investigated optical energy loss of CTO will add to the literature the optical properties of CTO. It should, however, be noted that the use of Cd-containing materials has significant ecological implications due to the toxic and persistent nature of Cd in the environment. While Cd-based compounds are employed in various technologies, including batteries, pigments, solar cells, and coatings, their potential for environmental contamination and health risks raises concerns. Since this study did not explore the electrical properties of CTO, which are also crucial in optoelectronic and photovoltaic applications, the computational study of the electrical properties of CTO can form the basis for further studies.

Funding: This project was funded by KAU Endowment (WAQF) at King Abdulaziz University, Jeddah, under grant no. (WAQF: 303-130-2024). The author, therefore, acknowledges with thanks WAQF and the Deanship of Scientific Research (DSR) for the technical and financial support.

Data Availability Statement: The data presented in this study are available in the article.

Conflicts of Interest: The author declares no conflicts of interest.

References

1. Salim, E.; Ismail, R.; Fakhri, M.; Rasheed, B.; Salim, Z. Synthesis of cadmium oxide/Si heterostructure for two-band sensor application. *Iran. J. Sci. Technol. Trans. A Sci.* **2018**, *43*, 1337–1343. [CrossRef]

2. Jamarkattel, M.; Phillips, A.; Bastola, E.; Neupane, S.; Li, D.; Yan, Y.; Ellingson, R.; Heben, M. Enabling High efficiency, flexible, and lightweight CdTe solar cells with a cadmium stannate transparent conducting oxide. In Proceedings of the 2023 IEEE 50th Photovoltaic Specialists Conference (PVSC), San Juan, PR, USA, 11–16 June 2023; pp. 1–3. [CrossRef]
3. Meysing, D.; Burst, J.; Rance, W.; Reese, M.; Barnes, T.; Gessert, T.; Wolden, C. The influence of cadmium sulfide and contact annealing configuration on the properties of high-performance cadmium stannate. *Sol. Energy Mater. Sol. Cells* **2013**, *117*, 300–305. [CrossRef]
4. Martínez-Saucedo, G.; Castanedo-Pérez, R.; Torres-Delgado, G.; Márquez-Marín, J.; Zelaya-Ángel, O. Cuprous oxide/cadmium stannate heterojunction diodes obtained by dip-coating method. *J. Alloys Compd.* **2019**, *774*, 153–159. [CrossRef]
5. Velásquez, C.; Campero, A.; Ortiz, A. Cadmium Stannate Thin Films Prepared by Sol-Gel Process. In *Emerging Fields in Sol-Gel Science and Technology*; López, T.M., Avnir, D., Aegerter, M., Eds.; Springer: Boston, MA, USA, 2003; pp. 317–321. [CrossRef]
6. Ongwen, N.; Oduor, A.; Ayieta, E. Effect of concentration of reactants on the optical properties of iron—Doped cadmium stannate thin films deposited by spray pyrolysis. *Am. J. Mater. Sci.* **2019**, *9*, 1–7.
7. Wu, X.; Coutts, T.; Mulligan, W. Properties of transparent conducting oxides formed from CdO and ZnO alloyed with SnO_2 and In_2O_3. *J. Vac. Sci. Technol.* **1997**, *15*, 1057–1062. [CrossRef]
8. Saeed, M.; Alshammari, Y.; Majeed, S.; Al-Nasrallah, E. Chemical vapor deposition of graphene—Synthesis, characterization, and applications: A review. *Molecules* **2020**, *25*, 3856. [CrossRef] [PubMed]
9. Soussi, A.; Haounati, R.; Ait hssi, A.; Taoufiq, M.; Baoubih, S.; Jellil, Z.; El hankari, S.; Elfanaoui, A.; Markazi, R.; Ihlal, A. Investigating structural, morphological, electronic, and optical properties of SnO_2 and Al-doped SnO_2: A combined DFT calculation and experimental study. *Phys. B Condens. Matter* **2024**, *690*, 416242. [CrossRef]
10. Gudmundsson, J.; Anders, A.; Von Keudell, A. Foundations of physical vapor deposition with plasma assistance. *Plasma Sources Sci. Technol.* **2022**, *31*, 083001. [CrossRef]
11. Sakthivel, P.; Murugan, R.; Asaithambi, S.; Karuppaiah, M.; Vijayaprasath, G.; Rajendran, S.; Hayakawa, Y.; Ravi, G. Studies on optoelectronic properties of magnetron sputtered cadmium stannate (Cd_2SnO_4) thin films as alternative TCO materials for solar cell applications. *Ceram. Int.* **2018**, *44*, 2529–2538. [CrossRef]
12. Ongwen, N.; Ogam, E.; Fellah, Z.E.A.; Mageto, M.; Othieno, H.; Otunga, H. Thermal properties and pressure-dependent elastic constants of cadmium stannate as a substrate for MEMS: An ab initio study. *Phys. B Condens. Matter* **2023**, *651*, 414599. [CrossRef]
13. Ongwen, N.; Ogam, E.; Otunga, H. Ab initio study of elastic properties of orthorhombic cadmium stannate as a substrate for the manufacture of MEMS devices. *Mater. Today Commun.* **2021**, *26*, 101822. [CrossRef]
14. Stoke, J.; Beach, J.; Bradford, W.; Ohno, T. Electrical and optical properties of magnetron sputtered Cd_2SnO_4 transparent conducting oxide thin films for use in CdTe solar devices. *Thin Solid Films* **2014**, *562*, 254–259. [CrossRef]
15. Bhuvaneswari, P.; Velusamy, P.; Babu, R.; Babu, M.; Ramamurthi, K.; Arivanandhan, M. Effect of fluorine doping on the structural, optical and electrical properties of spray deposited cadmium stannate thin films. *Mater. Sci. Semicond. Process.* **2013**, *16*, 1964–1970. [CrossRef]
16. Tang, M.; Shang, J.; Zhang, Y. Oxygen vacancy and doping atom effect on electronic structure and optical properties of Cd_2SnO_4. *RSC Adv.* **2018**, *8*, 640–646. [CrossRef] [PubMed]
17. Johannes, K.; Georg, S. What are structural properties? *Philos. Math.* **2018**, *26*, 295–323. [CrossRef]
18. Jeyadheepan, K.; Sanjeeviraja, C. Preparation and crystal structures of some AIVB2IIO4 compounds: Powder X-ray diffraction and Rietveld analysis. *J. Chem.* **2014**, *2014*, 245918. [CrossRef]
19. Bowden, M.E.; Cardile, C.M. Structures of orthorhombic and cubic dicadmium stannate by Rietveld Refinement. *Powder Diffr.* **1990**, *5*, 36–40. [CrossRef]
20. Trömel, M. Die kristallstruktur der verbindungen vom Sr_2PbO_4-typ. *Z. Anorg. Allg. Chem.* **1969**, *371*, 237–247. [CrossRef]
21. Zasimchuk, E.; Turchak, T.; Chausov, N. Hydrodynamic plastic flow in metal materials. *Results Mater.* **2020**, *6*, 100090. [CrossRef]
22. Raviendra, D.; Sharma, J.K. Electroless deposition of cadmium stannate, zinc oxide, and aluminum-doped zinc oxide films. *J. Appl. Phys.* **1985**, *58*, 838–844. [CrossRef]
23. Lakshmi, A.A.; Siva, V.; Pandiarajan, J.; Lawrence, B.; Prithivikumaran, N.; Jeyakumaran, N. Antibacterial activity of cadmium stannate nanoparticles synthesized by chemical precipitation method. *IOSR J. Appl. Phys.* **2022**, *14*, 1–6.
24. Zhu, Z.; Du, Z.; Liu, X.; Zhang, Y.; Wu, Q.; Lin, X. Cadmium stannate conductive layer with high optical transmittance and tunable work function. *Mater. Res. Express* **2021**, *8*, 016410. [CrossRef]
25. Yadav, M.K.; Sanyal, B. First-principles study of thermoelectric properties of CuI. *Mater. Res. Express* **2014**, *1*, 015708. [CrossRef]
26. Wan, Z.; Wang, Q.; Liu, D.; Liang, J. Effectively improving the accuracy of PBE functional in calculating the solid band gap via machine learning. *Comput. Mater. Sci.* **2021**, *198*, 110699. [CrossRef]
27. Viñes, F.; Lamiel-García, O.; Ko, K.; Lee, J.; Illas, F. Systematic study of the effect of HSE functional internal parameters on the electronic structure and band gap of a representative set of metal oxides. *J. Comput. Chem.* **2017**, *38*, 781–789. [CrossRef]
28. Mohammad, M.T.; Ghafor, W.A.A. Optical properties of cadmium stannate thin film prepared by pyrolytic process. *Solid State Commun.* **1989**, *72*, 1043–1046. [CrossRef]

29. Zheng, F.; Tao, J.; Rappe, A. Frequency-dependent dielectric function of semiconductors with application to physisorption. *Phys. Rev. B* **2016**, *95*, 035203. [CrossRef]
30. Petzelt, J.; Rychetský, I. *Dielectric Function, Reference Module in Materials Science and Materials Engineering*; Elsevier: Amsterdam, The Netherlands, 2016. [CrossRef]
31. Cazaux, J.; Perrin, J.; Soukiassian, P. Interband Transitions in Some Layered Chalcogenide Semiconductors. In Proceedings of the 12th International Conference on the Physics of Semiconductors, Stuttgart, Germany, 15–19 July 1974; Pilkuhn, M.H., Ed.; pp. 631–636. [CrossRef]
32. Coffeen, W.W. Ceramic and dielectric properties of the stannates. *J. Am. Ceram. Soc.* **1953**, *36*, 207–214. [CrossRef]
33. Salama, A.H.; Youssef, A.M.; Abbas, H.A.; Hammad, F.F. Comparison of the Electrical Properties for Undoped and Doped Indium Tin Oxide with Nanometal Oxides. *Interceram Int. Ceram. Rev.* **2016**, *65*, 179–186. [CrossRef]
34. Chang, T.; Kim, J.; Kang, S.; Kim, H.; Kim, D.; Lee, Y.; Shin, J. Broadband giant-refractive-index material based on mesoscopic space-filling curves. *Nat. Commun.* **2016**, *7*, 12661. [CrossRef] [PubMed]
35. Yurov, V.; Bushuev, E.; Popovich, A.; Bolshakov, A.; Ashkinazi, E.; Ralchenko, V. Near-infrared refractive index of synthetic single crystal and polycrystalline diamonds at high temperatures. *J. Appl. Phys.* **2017**, *122*, 243106. [CrossRef]
36. Gorelick, S.; Marco, A. Refractive micro-lenses and micro-axicons in single-crystal lithium niobate. *Opt. Express* **2018**, *26*, 32324–32331. [CrossRef] [PubMed]
37. Morford, R.; Mercado, R.; Planje, C.; Flaim, T. High refractive index photocurable resins. In *Organic Photonic Materials and Devices VII*; SPIE: San Jose, CA, USA, 2005; Volume 5724. [CrossRef]
38. Ueda, K.; Sonobe, O.; Chiba, H.; Sato, Y. Observation of continuum absorption spectra in far wings of the Yb resonance line broadened by He, Ne, Ar, Kr, Xe, and Yb. *J. Chem. Phys.* **1991**, *95*, 8083–8088. [CrossRef]
39. Sid, A. Nonlinear inverse bremsstrahlung absorption in laser-fusion plasma corona. *Phys. Plasmas* **2003**, *10*, 214–219. [CrossRef]
40. Agnihotri, O.; Gupta, B.; Sharma, A. Optical-absorption edge in cadmium stannate selective coatings. *J. Appl. Phys.* **1978**, *49*, 4540–4542. [CrossRef]
41. Ongwen, N.; Oduor, A.; Ayieta, E. Effect of deposition temperature on the optical properties of iron-doped cadmium stannate thin films deposited by spray pyrolysis. *IJSTRE Int. J. Sci. Tech. Res. Eng.* **2019**, *4*, 38–48.
42. Allan, L.; Mulwa, W.M.; Mapasha, R.E.; Mwabora, J.M.; Musembi, R.J. First principle study of $ATiO_3$ (A = Ti, Sr) materials for photovoltaic applications. *J. Mol. Model.* **2024**, *30*, 32. [CrossRef] [PubMed]
43. Vandewal, K.; Benduhn, J.; Nikolis, V. How to determine optical gaps and voltage losses in organic photovoltaic materials. *Sustain. Energy Fuels* **2018**, *2*, 538–544. [CrossRef]
44. Crystallography Open Database. Available online: http://www.crystallography.net/cod/1522049.html (accessed on 20 November 2024).
45. Giannozzi, P.; Baroni, S.; Bonini, N.; Calandra, M.; Car, R.; Cavazzoni, C.; Ceresoli, D.; Chiarotti, G.L.; Cococcioni, M.; Dabo, I.; et al. QUANTUM ESPRESSO: A modular and open-source software project for quantum simulations of materials. *J. Phys. Condens. Matter* **2009**, *21*, 395502. [CrossRef] [PubMed]
46. Monkhorst, H.J.; Pack, J.D. Special points for Brillouin zone integration. *Phys. Rev. B* **1976**, *13*, 5188. [CrossRef]
47. Suleiman, M.S.H.; Molepo, M.P.; Joubert, D.P. A theoretical investigation of structural, electronic and optical properties of bulk copper nitrides. *J. Alloys Compd.* **2018**, *753*, 576–585. [CrossRef]
48. Wafula, J.W. Structural, elastic, electronic, optical and thermal properties of YMAu (M = Si or Ge or Sn) Half-Heusler compounds; A DFT study. *Results Mater.* **2023**, *19*, 100413. [CrossRef]

Disclaimer/Publisher's Note: The statements, opinions and data contained in all publications are solely those of the individual author(s) and contributor(s) and not of MDPI and/or the editor(s). MDPI and/or the editor(s) disclaim responsibility for any injury to people or property resulting from any ideas, methods, instructions or products referred to in the content.